ACS APPLIED MATERIALS & INTERFACES

Research Article

www.acsami.org

Adsorption Properties of *p*-Methyl Red Monomeric-to-Pentameric Dye Aggregates on Anatase (101) Titania Surfaces: First-Principles Calculations of Dye/TiO_2 Photoanode Interfaces for Dye-Sensitized Solar Cells

Lei Zhang[†] and Jacqueline M. Cole*[,†,‡]

[†]Cavendish Laboratory, University of Cambridge, J. J. Thomson Avenue, Cambridge, CB3 0HE, U.K.

[‡]Argonne National Laboratory, 9700 South Cass Avenue, Argonne, Illinois 60439, United States

Supporting Information

ABSTRACT: The optical and electronic properties of dye aggregates of *p*-methyl red on a TiO_2 anatase (101) surface were modeled as a function of aggregation order (monomer to pentameric dye) via first-principles calculations. A progressive red-shifting and intensity increase toward the visible region in UV−vis absorption spectra is observed from monomeric-to-tetrameric dyes, with each molecule in a given aggregate binding to one of the four possible TiO_2 (101) adsorption sites. The pentamer exhibits a blue-shifted peak wavelength in the UV−vis absorption spectra and less absorption intensity in the visible region in comparison; a corresponding manifestation of H-aggregation occurs since one of these five molecules cannot occupy an adsorption site. This finding is consistent with experiment. Calculated density of states (DOS) and partial DOS spectra reveal similar dye···TiO_2 nanocomposite conduction band characteristics but different valence band features. Associated molecular orbital distributions reveal dye-to-TiO_2 interfacial charge transfer in all five differing aggregate orders; meanwhile, the level of intramolecular charge transfer in the dye becomes progressively localized around its azo- and electron-donating groups, up to the tetrameric dye/TiO_2 species. Dye adsorption energies and dye coverage levels are calculated and compared with experiment. Overall, the findings of this case study serve to aid the molecular design of azo dyes toward better performing DSSC devices wherein they are incorporated. In addition, they provide a helpful example reference for understanding the effects of dye aggregation on the adsorbate···TiO_2 interfacial optical and electronic properties.

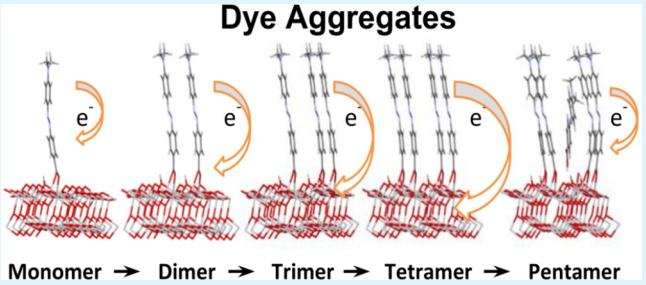

KEYWORDS: *dye-sensitized solar cells, aggregation, organic dye, optoelectronic materials*

INTRODUCTION

The dye-sensitized solar cell (DSSC) has rapidly developed since 1991.[1−4] It has exhibited potential to disrupt the silicon-based solar cell industry owing to its lower cost and high efficiency.[5] In DSSCs, dyes are critical to absorb light and convert it into electrical power, when in contact with TiO_2 substrate. Compared with organometallic dyes based on zinc, ruthenium, and perovskite, organic dyes enjoy various advantages such as easier synthesis, molecular tunability, and abundance.[6−8]

Dye aggregate formation in a self-assembled monolayer (SAM) has been demonstrated to affect strongly the electronic and optical properties of organic chromophores in the DSSC device.[9−11] Methods that enhance solar cell device performance by manipulating the nature of the dye aggregates in DSSCs have been facilitated by insights from first-principles calculations.[12−16] Density functional theory (DFT)-based methods are a natural choice for modeling the dye/TiO_2 interface of a DSSC, based on their high record of success in reproducing experimental results and unveiling underlying electronic and optoelectronic mechanisms.[17] Nevertheless, local van der Waals interactions have historically been neglected in traditional DFT methods. Recently, the use of dispersion corrections has been advocated to account for the van der Waals interactions among molecules,[18−20] and it is crucial to consider dispersion in this study involving aggregation of molecules. Ab initio dimeric aggregation calculations on TiO_2 have been performed by De Angelis et al. on a TiO_2 cluster that features a (101) surface, the preferred and dominant site of dye adsorption.[12,21,22] However, a more complete view of organic dye aggregation on TiO_2, presenting dyes progressively as monomeric, dimeric, trimeric, tetrameric and pentameric adsorbates, has not been reported using first-principles calculations. In addition, previous studies on aggregation are based on an isolated TiO_2 cluster, where the

Received: May 2, 2014
Accepted: August 22, 2014
Published: August 22, 2014

   dx.doi.org/10.1021/am502687k | ACS Appl. Mater. Interfaces 2014, 6, 15760−15766

"edge effect" is often exaggerated because of the finite substrate size. This edge effect could be circumvented by employing a periodic geometric model that embraces plane wave based density functional theory (DFT) calculations.[23,24] This study serves to bridge these gaps by performing calculations that systematically probe monomeric-to-pentameric dye adsorbates on TiO_2, thus extending our theoretical understanding of organic dye aggregation onto TiO_2. In particular, their density of states, molecular orbital distributions, optical absorption spectra, adsorption energies, and levels of dye coverage onto the (101) TiO_2 surface are probed.

Azo dyes form one of the largest categories of industrial dyes due to light fastness, lower cost and universal availability. They have been incorporated into DSSCs recently;[25,26] although the resulting device performance achieved so far is modest, a better theoretical understanding of its dye···TiO_2 interface stands to direct the molecular design of azo dyes toward competitive operational device function. Azo dyes also exhibit interesting surface and interface phenomena, when manifest as an SAM, such as water uphill movement and photoswitching properties,[27,28] where aggregation can potentially play important role.[29]

In this paper, the azo dye (*E*)-4-((4-(dimethylamino)-phenyl)diazenyl)benzoic acid, more commonly known as *p*-methyl red (**1**) is used as the case study to probe the effect of organic dye aggregation, up to pentameric species, at the TiO_2 anatase (101) surface. The choice of this case study arises from prior confirmation that para-substituted azo dyes function better than the ortho- or meta-substituted azo dyes.[25] It has been proposed from experiments that H-aggregation dominates for such a dye at the metal oxide surface, evidenced by blue-shifted UV−vis spectra of the dye adsorbed onto the TiO_2 substrate.[30]

Scheme 1. Molecular Structure of 4-[2-[4-(Dimethylamino)phenyl]diazenyl]-benzoic Acid or *p*-Methyl Red

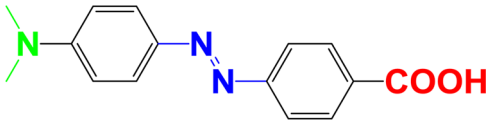

COMPUTATIONAL DETAILS

To assess the dye aggregation effects of *p*-methyl red on a TiO_2 substrate, a large anatase (101) surface (10.42 Å × 15.20 Å) twice the size as that studied by Vittadini et al.[31] was constructed. The thickness of each slab was ∼7 Å. A 20 Å vacuum layer was placed on top of the surface to ensure minimal interactions between slabs. Geometric optimization was performed in CASTEP[32] and the structure was visualized in Materials Studio and Mercury.[33] The geometric optimization was performed at the Γ-point, which provides sufficient Brillouin zone sampling due to the large system size. The bottom layer of the TiO_2 slab was constrained during geometric optimization, while all other layers were allowed to relax. The cutoff energy was set to 370 eV, using ultrasoft pseodopotentialsand the PBE functional. van der Waals interactions were considered by performing DFT-D calculations using the Tkatchenko−Scheffler (TS) scheme.[34] The geometrical energy, force and displacement converged within fair limits (5×10^{-6} eV, 0.04 eV/Å and 4×10^{-3} Å, respectively). Density of states (DOS) and partial density of states (PDOS) spectra were obtained at the optimized geometry.

The same pseudopotential and PBE functional were used to calculate the optical properties of this dye/TiO_2 nanocomposite, where the cutoff energy was 340 eV. Thirty-two special *k* points in the Brillouin zone were summed to derive these optical properties from calculating the dielectric constant.

Four dye···TiO_2 adsorption sites, with 5-fold coordinated and unsaturated titanium atoms, namely, a, b, c, and d in Figure 1, are

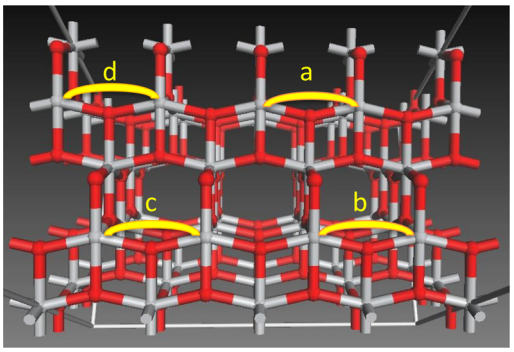

Figure 1. Top view of the unit cell with the (101) anatase surface exposed. Four anchoring positions on the TiO_2 anatase (101) surface are labeled as a, b, c, and d.

available on the (101) surface of the anatase unit cell. Based on these four adsorption sites, seven structures ("a", "ab", "ac", "ad", "abc", "abcd", and "poor") were evaluated in the study to probe the aggregation effects, in addition to the free dye and the bare TiO_2 slab. "a" has monomeric adsorption at site a; "ab" has dimeric aggregates at both a and b sites; similarly, "ac" exhibits dimeric aggregation at both a and c sites, while "ad" displays dimeric aggregates at both a and d sites; "abc" shows trimeric aggregation at a, b and c sites; and "abcd" has tetrameric aggregates with dye adsorption taking up all available sites (a, b, c, and d). A pentameric adsorbate was also modeled; this was termed "poor" since the additional (fifth) adsorbed azo dye in this system laid irregularly relative to the other four dyes, having been placed in the supercell of "abcd". This irregular positioning of the fifth dye in the "poor" structure occurs because the unsaturated 5-fold titanium atoms, at a, b, c, and d positions on the TiO_2 surface, have been used up and so are not available for the fifth azo molecule; thus, a poor alignment and inefficient adsorption of this fifth dye results. For the geometrical optimization of "poor", a number of initial guesses for the position of the fifth molecule were tested, including placing: the dimethylamine group near the surface, the molecule horizontally on the slab, the azo group near the TiO_2 surface and moving to other positions for the extra group; however, all of them failed to converge, except for the structure of "poor" described in this work. The adsorption of the fifth molecule, manifest in the optimized structure, is stabilized by a "hydrogen bond" between a TiO_2 anatase (101) surface oxygen atom and an oxygen atom in the carbonyl group of the dye (Figure 2).

The average adsorption energy between an organic dye and the TiO_2 substrate in a dye/TiO_2 structure is expressed as

$$E_{\text{adsorption}} = (n \times E_{\text{dyes}} + E_{\text{TiO}_2} - E_{\text{dyes/TiO}_2})/n$$

where *n* is the number of dye molecules adsorbed (*n* = 1 for "a", *n* = 2 for "ab", *n* = 3 for "abc", *n* = 4 for "abcd", and *n* = 5 for "poor"). The first term in the parentheses denotes the total energy of isolated dyes; the second term represents the total energy of the bare TiO_2 slab; and the third term stands for the total energy of the optimized dye/TiO_2 system.

RESULTS AND DISCUSSION

Structure of dye Adsorbates on a (101) TiO_2 Surface. In the optimized dye/TiO_2 structures (Figure 2), the separation between the oxygen atoms in the carboxylic acid groups and surface titanium ranges from 2.02 to 2.12 Å, which is similar as that seen between formic acid and anatase.[31] The two C−O

dx.doi.org/10.1021/am502687k | ACS Appl. Mater. Interfaces 2014, 6, 15760−15766

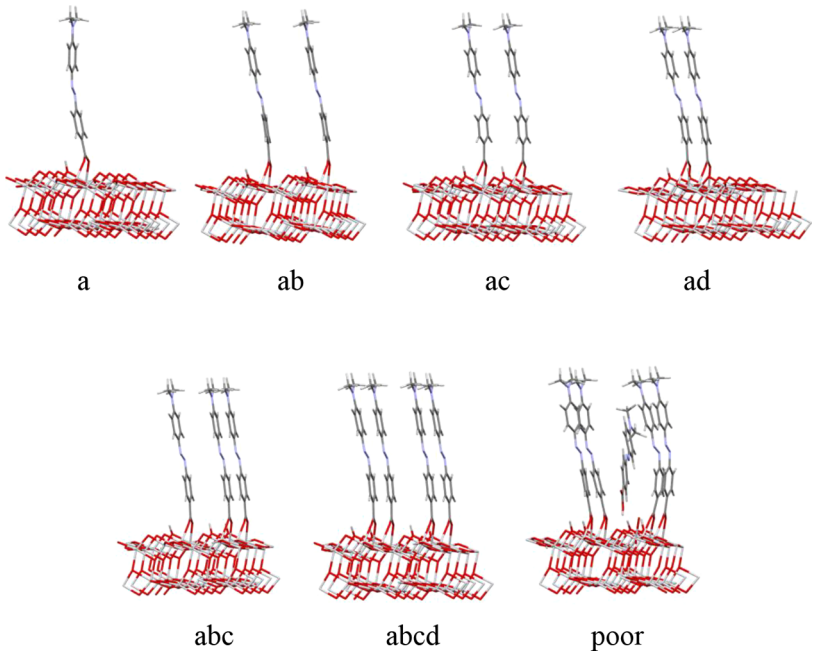

Figure 2. Optimized structural geometries of different dye aggregates, adsorbed as a monomer (a), dimer (ab, ac, ad), trimer (abc), tetramer (abcd), or pentamer (poor); the latter is so named owing to the poor ability of one of its dye molecules to adsorb onto TiO_2 since all four of its natural anchoring points are occupied.

bonds (C═O vs C−O) in the carboxylate group of all the adsorbates appear to have almost equivalent lengths (1.28−1.30 Å), except the unadsorbed molecule in the "poor", due to its undissociative nature that maintains the asymmetry of bond lengths in carboxylic acid group. The bond length of the azo group is essentially invariant among different aggregates (1.30−1.31 Å). Conjugation of a molecule is important in order to ensure low-energy charge-separation.[35] The level of conjugation can be quantified by considering the ring-to-ring interplanar angles within the molecule.[25] The average torsion angles between the two phenyl rings of an azo molecule are similar for the aggregates: 12° (a), 11° (ab), 11° (ac), 11° (ad), 12° (abc), 12° (abcd), and 17° (poor). The "poor" presents slightly larger torsion angles between phenyl rings, indicating that they exhibit less intramolecular charge transfer[25] compared with other structures; this is consistent with the trend observed in the UV−vis absorption spectra (vide infra). Compared with the other aggregates, the "poor" structure bears distorted dye molecules (Figure 2); this appears to be due to steric repulsion caused by the extra molecule being introduced into a limited space with no suitable TiO_2 surface anchoring point.

DOS and PDOS. DOS and PDOS spectra (Figure 3) show that Ti-3d orbitals are largely responsible for populating the bottom of the conduction bands of TiO_2 and dye/TiO_2. Having applied dispersion corrections, the conduction bands of PDOS for all the adsorbed structures are similar, while, for the valence bands, PDOS show increasing contributions from nitrogen atoms for higher degrees of aggregation. The top of the valence bands of TiO_2 primarily constitute O-2p orbital features while those of the dye/TiO_2 nanocomposite mainly feature contributions from C-2p and N-2p in the organic moiety. The O-s, Ti-s, and Ti-p orbitals manifest predominantly in the deep region of the valence bands (Supporting Information Figure S1). Upon dye adsorption, the band gap, defined here as the energy difference between valence band maximum (VBM) and conduction band minimum (CBM) at the Γ point, decreases, compare the energy of the bare TiO_2 slab (2.8 eV) versus that of the dye/TiO_2 structures (0.8−1.2 eV) shown in Supporting Information Table S1. The band gap should be used with caution as the new "valence band" of the dye/TiO_2 system comprises contributions from dye orbitals rather than the metal oxide. Nevertheless, this small band is important in DSSCs, as the electron essentially originates from this "small valence band" where organic dyes primarily contribute. This gap reduction indicates the effectiveness of organic dyes on modifying the electronic properties of the metal oxide.

Optical Properties. The optical absorption properties of the dye/TiO_2 slab are dependent upon the different forms of aggregates (Figure 4). There are two bands in the UV−vis region: band 1 corresponds to the spectra in the near UV region from ∼300 to 400 nm while band 2 corresponds to the spectra in the visible region near 600 nm, Compared with the bare TiO_2 substrate, the monomeric adsorption structure "a" exhibits a red-shifted light absorption peak and higher absorptivity in band 1. The dimeric adsorption modes "ab", "ac", and "ad" present further red shifting compared with "a"; each of these modes possess similar UV/vis absorption spectra with each other. The peak wavelength and peak intensity of the two bands in the UV/vis absorption spectra have been summarized in Supporting Information Table S2. Generally, in band 1, there is monotonical red-shift, by 3−6 nm, from a lower degree of aggregation to the next higher degree (for example, the red shift is 6 nm from "abc" to "abcd"). In addition, the intensity of band 1 increases monotonically by 100−600 cm^{-1} from a lower degree of aggregation to the next higher degree (for example, the intensity increases ∼600 cm^{-1} from "abc" to "abcd"). This red-shifted trend, as a function of increasing number of adsorbed dye adsorbate molecules, is disrupted, when the fifth molecule is introduced to form the pentamer, "poor"; that is, the "poor" dye/TiO_2 structure exhibits a blue-shift in absorption spectrum, compared with that

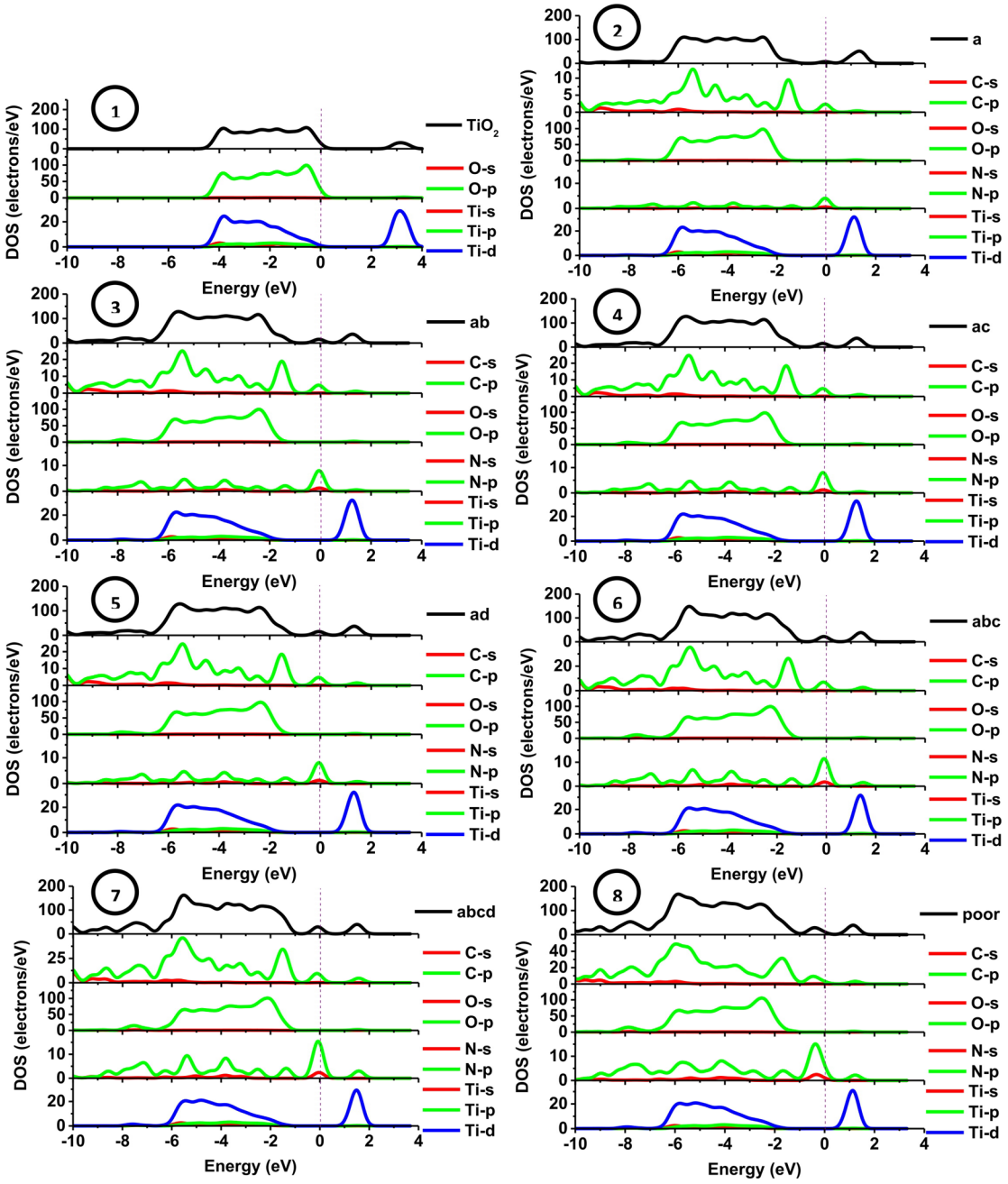

Figure 3. DOS plots of bare "TiO_2" (1), "a" (2), "ab" (3), "ac" (4), "ad" (5), "abc" (6), "abcd" (7), and "poor" (8) structures (top spectra in each plot; black), and PDOS contributions (from C, O, N and Ti s (red), p (green) and, in the case of Ti, d (blue) orbitals. The vertical dotted lines correspond to the Fermi energy, which is set to 0 eV.

of "abcd". There is also an intensity decrease, by ~3000 cm^{-1}, from the tetramer to the pentamer.

For band 2, although a blue-shift manifests from monomer to tetramer in this region of the light absorption spectra, the intensity nevertheless increases by 2000−5000 cm^{-1} for the next higher degree of aggregate. As a result, the blue shift in band 2 from the monomer-to-tetramer sequence is not obvious in the UV−vis absorption spectra, owing to the blue-shifted peak wavelength being reduced by the rise in intensity. This leads to light absorption spectra with blue-shifts toward the UV region and insufficient absorption in the visible region, when the dyes are adsorbed on TiO_2, compared with solution where aggregation is not severe. These results indicate that the aggregates should benefit DSSC light-harvesting performance up to tetrameric species. In contrast, "poor" is not ideal for DSSC application since the intensity decreases by ~3000 cm^{-1}, from tetramer to "poor". This finding is compatible with experimental results, where H-aggregation exhibits blue-shifted absorption spectra and inferior absorption intensity in the visible region for azo dyes on TiO_2.[30]

Orbital Distributions. The orbital distributions of VBM − 2, VBM − 1, VBM, CBM, and CBM + 1 (Figure 5) reveal that the valence bands are localized within the dye molecule while the conduction bands are localized inside the metal oxide. This usually indicates favorable charge injection in the photoanode of a DSSC.[24] As the degree of aggregation increases, progressing from monomeric to tetrameric dye adsorbates in the dye/TiO_2 structures, their electronic distributions in the

dx.doi.org/10.1021/am502687k | ACS Appl. Mater. Interfaces 2014, 6, 15760−15766

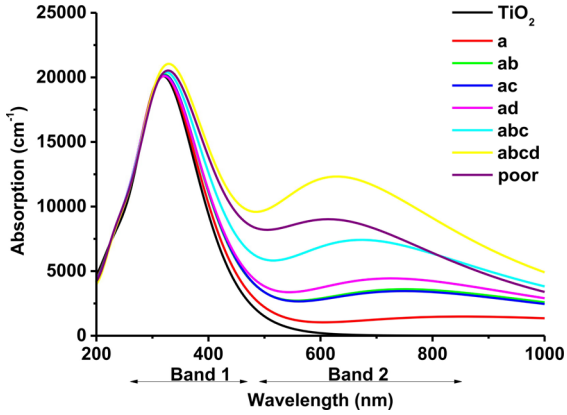

Figure 4. UV−vis absorption spectra of "a", "ab", "ac", "ad", "abc", "abcd", and "poor" *p*-methyl red dye adsorbates on TiO_2, predicted by first-principles calculations, demonstrating an increase in band 2 intensity as a function of progressively higher-order aggregates, with the partial exception of the 5th-order aggregate, "poor". An analogous spectrum corresponding to the bare TiO_2 is also provided, for reference.

valence band become more localized in the region surrounding the azo group (−N═N−). The majority of the valence bands in the pentamer are distributed in the poorly adsorbed fifth molecule for "poor"; this is perhaps not surprising given that this slantingly aligned molecule presents a closer dye cation-TiO_2 separation to the others, and it is therefore more prone to electron recombination.[36]

Dye Adsorption Energies and Dye Coverage on the TiO_2 (101) Surface. Different dye aggregate structures exhibit varying adsorption energies (Table 1). The adsorption energies for different aggregates follow the ranking: monomer < dimer < trimer < tetramer < pentamer. The pentamer displays the largest adsorption energy because of its densely packed aromatic system, which is stabilized by the dispersion correction. The extent of dye coverage increases monotonically throughout the series, from 0.1 nmol/cm^2 for "a" to 0.52 nmol/cm^2 for "poor". Compared with experimentally determined dye adsorption take-up (147 nmol/cm^2),[30] the dye coverage estimated here is particularly small; this is attributed to the inherent limitation of the periodic slab model, without

Table 1. Estimated Adsorption Energies and Dye Coverage Levels on the (101) TiO_2 Surface for Different Adsorbed Dye Structures

	a	ab	ac	ad	abc	abcd	poor
adsorption (eV)	−0.16	0.66	0.47	0.49	0.84	1.03	1.55
dye coverage (nmol/cm^2)	0.10	0.21	0.21	0.21	0.31	0.42	0.52

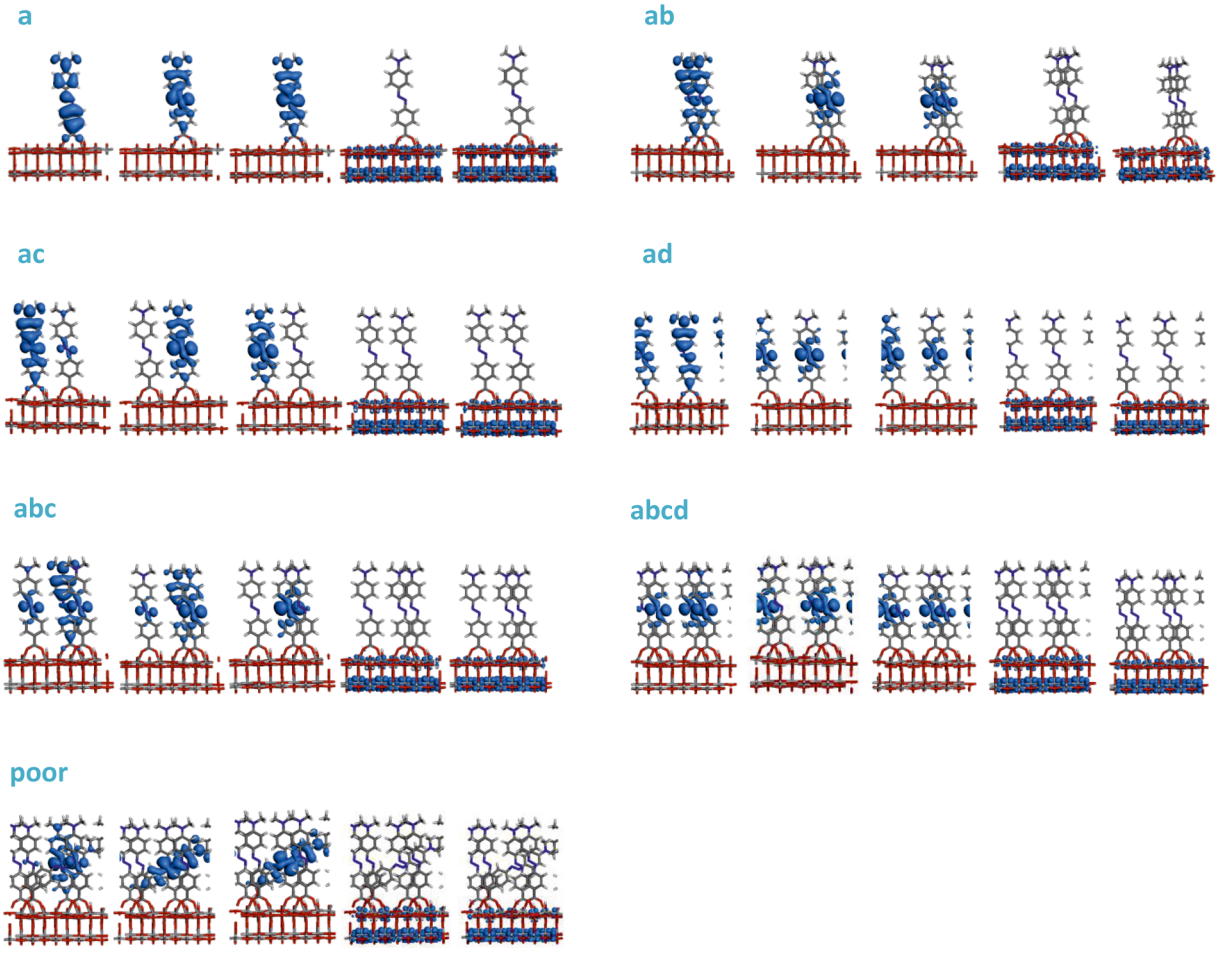

Figure 5. Orbital distributions of the dye/TiO_2 systems. Five orbitals are presented from left to right of each structure: VBM-2, VBM-1, VBM, CBM, and CBM + 1.

dx.doi.org/10.1021/am502687k | ACS Appl. Mater. Interfaces 2014, 6, 15760−15766

considering a mesoporous TiO_2 structure as the real scenario. Nevertheless, the calculated trend of increasing dye coverage as a function of higher aggregation, from monomer to pentamer, is expected to be consistent with experiment.

CONCLUSIONS

The extent of dye aggregation of the *p*-methyl red dye on the (101) surface of TiO_2 has been demonstrated to affect the electronic and optical properties of the photoanode for DSSCs. Our understanding of dye aggregation in DSSCs for this chemical family of dyes has been enhanced by considering not only the lower degree of dye aggregation such as dimers, as per previous reports, but also higher-order aggregation such as trimers, tetramers and pentamers. Dyes ranging from monomer to tetrameric aggregates exhibit minimal structural differences, while the pentameric form differs; there, the fifth molecule that is added to the aggregate to form the pentamer is squeezed into a limited space between the existing four adsorbed molecules, since there are no adsorption sites remaining for it to anchor strongly to TiO_2; as such, it might exert steric forces onto other molecules. DOS and PDOS analyses indicate that the monomeric- pentameric dye adsorbates on TiO_2 have greater contributions from nitrogen atoms in the top of the valence band. Molecular orbital distributions in the top of valence band of dye/TiO_2 are mostly populated in the vicinity of the azo group and the electron donor region, while they are localized with the metal oxide at the bottom of the conduction band. Dye aggregation effects are nicely evidenced in the calculated UV/vis absorption spectra, where progressively higher degrees of aggregation demonstrate monotonic red shifting and higher absorption intensity in the simulated spectra, up to the tetrameric form. The blue shift and lower light absorption intensity throughout the UV−vis regime observed in the pentamer suggests that the poorly adsorbed molecules in this adsorbate cannot be neglected in solar cell design; indeed, there is a consistent agreement with experimental UV−vis absorption spectral features encountered in the photoanode fabrication steps for certain organic dyes. The large discrepancy of calculated versus experimentally determined dye coverage levels (by two orders of difference) may arise from an underestimation in the surface area of the (101) TiO_2, owing to the use of the periodic slab model, as well as from the assumption of monolayer dye adsorption used in this study. Nonetheless, the consistent monotonic increase in the extent of dye coverage from monomeric-to-pentameric adsorbates is informative. In general terms, the overarching nature and trends in dye···TiO_2 interfacial adsorption, revealed by this case study, stand to be useful as an example reference for understanding the adsorption properties of this and other classes of dyes on TiO_2 anatase (101) surfaces, for DSSC applications.

ASSOCIATED CONTENT

Supporting Information

Details of DOS and PDOS spectra and energy band gaps for of "a", "ab", "ac", "ad", "abc", "abcd", and "poor" dye adsorbates and the peak wavelength and intensity of bare "TiO_2", "a", "ab", "ac", "ad", "abc", "abcd", and "poor". This material is available free of charge via the Internet at http://pubs.acs.org.

AUTHOR INFORMATION

Corresponding Author

*E-mail: jmc61@cam.ac.uk. Tel: +44 (0)1223 337470. Fax: +44 (0)1223 373536.

Author Contributions

The manuscript was written through contributions of all authors. All authors have given approval to the final version of the manuscript.

Notes

The authors declare no competing financial interest.

ACKNOWLEDGMENTS

J.M.C. thanks the Fulbright Commission for a U.K.−U.S. Fulbright Scholar Award, hosted by Argonne National Laboratory where work done was was supported by DOE Office of Science, Office of Basic Energy Sciences, under contract No. DE-AC02-06CH11357. The authors acknowledge computational support from the University of Cambridge High Performance Computing Cluster (HPC, Darwin).

REFERENCES

(1) O'Regan, B.; Grätzel, M. A Low-Cost, High-Efficiency Solar Cell Based on Dye-Sensitized Colloidal TiO_2 Films. *Nature* **1991**, *353*, 737−740.

(2) Grätzel, M. Dye-Sensitized Solar Cells. *J. Photochem. Photobiol., C* **2003**, *4*, 145−153.

(3) Grätzel, M. Recent Advances in Sensitized Mesoscopic Solar Cells. *Acc. Chem. Res.* **2009**, *42*, 1788−1798.

(4) Nazeeruddin, M. K.; De Angelis, F.; Fantacci, S.; Selloni, A.; Viscardi, G.; Liska, P.; Ito, S.; Takeru, B.; Grätzel, M. Combined Experimental and DFT-TDDFT Computational Study of Photoelectrochemical Cell Ruthenium Sensitizers. *J. Am. Chem. Soc.* **2005**, *127*, 16835−16847.

(5) Mathew, S.; Yella, A.; Gao, P.; Humphry-Baker, R.; Curchod, B. F. E.; Ashari-Astani, N.; Tavernelli, I.; Rothlisberger, U.; Nazeeruddin, M. K.; Grätzel, M. Dye-Sensitized Solar Cells with 13% Efficiency Achieved through the Molecular Engineering of Porphyrin Sensitizers. *Nat. Chem.* **2014**, *6*, 242−247.

(6) Kim, S.; Lee, J. K.; Kang, S. O.; Ko, J.; Yum, J.-H.; Fantacci, S.; De Angelis, F.; Di Censo, D.; Nazeeruddin, M. K.; Grätzel, M. Molecular Engineering of Organic Sensitizers for Solar Cell Applications. *J. Am. Chem. Soc.* **2006**, *128*, 16701−16707.

(7) Jiao, Y.; Zhang, F.; Grätzel, M.; Meng, S. Structure−Property Relations in All-Organic Dye-Sensitized Solar Cells. *Adv. Funct. Mater.* **2013**, *23*, 424−429.

(8) Mishra, A.; Fischer, M. K. R.; Bäuerle, P. Metal-Free Organic Dyes for Dye-Sensitized Solar Cells: From Structure: Property Relationships to Design Rules. *Angew. Chem., Int. Ed.* **2009**, *48*, 2474−2499.

(9) Gadde, S.; Batchelor, E. K.; Weiss, J. P.; Ling, Y.; Kaifer, A. E. Control of H- and J-Aggregate Formation via Host−Guest Complexation Using Cucurbituril Hosts. *J. Am. Chem. Soc.* **2008**, *130*, 17114−17119.

(10) Kim, S.; An, T. K.; Chen, J.; Kang, I.; Kang, S. H.; Chung, D. S.; Park, C. E.; Kim, Y.-H.; Kwon, S.-K. H-Aggregation Strategy in the Design of Molecular Semiconductors for Highly Reliable Organic Thin Film Transistors. *Adv. Funct. Mater.* **2011**, *21*, 1616−1623.

(11) Numata, Y.; Islam, A.; Chen, H.; Han, L. Aggregation-Free Branch-Type Organic Dye with a Twisted Molecular Architecture for Dye-Sensitized Solar Cells. *Energy Environ. Sci.* **2012**, *5*, 8548.

(12) Pastore, M.; De Angelis, F. Aggregation of Organic Dyes on TiO_2 in Dye-Sensitized Solar Cells Models: An Ab Initio Investigation. *ACS Nano* **2010**, *4*, 556−562.

(13) Wu, Y.; Marszalek, M.; Zakeeruddin, S. M.; Zhang, Q.; Tian, H.; Grätzel, M.; Zhu, W. High-Conversion-Efficiency Organic Dye-Sensitized Solar Cells: Molecular Engineering on D−A−π-A Featured Organic Indoline Dyes. *Energy Environ. Sci.* **2012**, *5*, 8261.

(14) Galoppini, E. Linkers for Anchoring Sensitizers to Semiconductor Nanoparticles. *Coord. Chem. Rev.* **2004**, *248*, 1283−1297.

(15) Hirva, P.; Haukka, M. Effect of Different Anchoring Groups on the Adsorption of Photoactive Compounds on the Anatase (101) Surface. *Langmuir* **2010**, *26*, 17075−17081.
(16) Liu, X.; Cole, J. M.; Low, K. S. Molecular Origins of Dye Aggregation and Complex Formation Effects in Coumarin 343. *J. Phys. Chem. C* **2013**, *117*, 14723−14730.
(17) Labat, F.; Le Bahers, T.; Ciofini, I.; Adamo, C. First-Principles Modeling of Dye-Sensitized Solar Cells: Challenges and Perspectives. *Acc. Chem. Res.* **2012**, *45*, 1268−1277.
(18) Grimme, S. Density Functional Theory with London Dispersion Corrections. *Wiley Interdiscip. Rev.: Comput. Mol. Sci.* **2011**, *1*, 211−228.
(19) Sorescu, D. C.; Lee, J.; Al-Saidi, W. a; Jordan, K. D. CO_2 Adsorption on TiO_2(110) Rutile: Insight from Dispersion-Corrected Density Functional Theory Calculations and Scanning Tunneling Microscopy Experiments. *J. Chem. Phys.* **2011**, *134*, No. 104707.
(20) Ruiz, V. G.; Liu, W.; Zojer, E.; Scheffler, M.; Tkatchenko, A. Density-Functional Theory with Screened van Der Waals Interactions for the Modeling of Hybrid Inorganic-Organic Systems. *Phys. Rev. Lett.* **2012**, *108*, No. 146103.
(21) Agrawal, S.; Pastore, M.; Marotta, G.; Reddy, M. A.; Chandrasekharam, M.; De Angelis, F. Optical Properties and Aggregation of Phenothiazine-Based Dye-Sensitizers for Solar Cells Applications: A Combined Experimental and Computational Investigation. *J. Phys. Chem. C* **2013**, *117*, 9613−9622.
(22) Marotta, G.; Reddy, M. A.; Singh, S. P.; Islam, A.; Han, L.; De Angelis, F.; Pastore, M.; Chandrasekharam, M. Novel Carbazole−Phenothiazine Dyads for Dye-Sensitized Solar Cells: A Combined Experimental and Theoretical Study. *ACS Appl. Mater. Interfaces* **2013**, *5*, 9635−9647.
(23) Yu, Q.; Jin, L.; Zhou, C. Ab Initio Study of Electronic Structures and Absorption Properties of Pure and Fe^{3+}-Doped Anatase TiO_2. *Sol. Energy Mater. Sol. Cells* **2011**, *95*, 2322−2326.
(24) Liang, J.; Zhu, C.; Cao, Z. Electronic and Optical Properties of the Triphenylamine-Based Organic Dye Sensitized TiO_2 Semiconductor: Insight from First Principles Calculations. *Phys. Chem. Chem. Phys.* **2013**, *15*, 13844−13851.
(25) Zhang, L.; Cole, J. M.; Waddell, P. G.; Low, K. S.; Liu, X. Relating Electron Donor and Carboxylic Acid Anchoring Substitution Effects in Azo Dyes to Dye-Sensitized Solar Cell Performance. *ACS Sustainable Chem. Eng.* **2013**, *1*, 1440−1452.
(26) Zhang, L.; Cole, J. M. TiO_2-Assisted Photoisomerization of Azo Dyes Using Self-Assembled Monolayers: Case Study on para-Methyl Red Towards Solar-Cell Applications. *ACS Appl. Mater. Interfaces* **2014**, *6*, 3742−3729.
(27) Ichimura, K. Light-Driven Motion of Liquids on a Photoresponsive Surface. *Science* **2000**, *288*, 1624−1626.
(28) Browne, W. R.; Feringa, B. L. Light Switching of Molecules on Surfaces. *Annu. Rev. Phys. Chem.* **2009**, *60*, 407−428.
(29) Song, X.; Perlstein, J.; Whitten, D. G. Photoreactive Supramolecular Assemblies: Aggregation and Photoisomerization of Azobenzene Phospholipids in Aqueous Bilayers. *J. Am. Chem. Soc.* **1995**, *117*, 7816−7817.
(30) Zhang, L.; Cole, J. M.; Dai, C. Variation in Optoelectronic Properties of Azo Dye-Sensitized TiO2 Semiconductor Interfaces with Different Adsorption Anchors: Carboxylate, Sulfonate, Hydroxyl and Pyridyl Groups. *ACS Appl. Mater. Interfaces* **2014**, *6*, 7535−7546.
(31) Vittadini, A.; Selloni, A.; Rotzinger, F. P.; Grätzel, M. Formic Acid Adsorption on Dry and Hydrated TiO_2 Anatase (101) Surfaces by DFT Calculations. *J. Phys. Chem. B* **2000**, *104*, 1300−1306.
(32) Segall, M. D.; Lindan, P. J. D.; Probert, M. J.; Pickard, C. J.; Hasnip, P. J.; Clark, S. J.; Payne, M. C. First-Principles Simulation: Ideas, Illustrations, and the CASTEP Code. *J. Phys.: Condens. Matter* **2002**, *14*, 2717−2744.
(33) Macrae, C. F.; Edgington, P. R.; McCabe, P.; Pidcock, E.; Shields, G. P.; Taylor, R.; Towler, M.; van de Streek, J. Mercury: Visualization and Analysis of Crystal Structures. *J. Appl. Crystallogr.* **2006**, *39*, 453−457.
(34) Tkatchenko, A.; Scheffler, M. Accurate Molecular Van Der Waals Interactions from Ground-State Electron Density and Free-Atom Reference Data. *Phys. Rev. Lett.* **2009**, *102*, No. 073005.
(35) Brédas, J.-L.; Beljonne, D.; Coropceanu, V.; Cornil, J. Charge-Transfer and Energy-Transfer Processes in Pi-Conjugated Oligomers and Polymers: A Molecular Picture. *Chem. Rev.* **2004**, *104*, 4971−5004.
(36) Clifford, J. N.; Palomares, E.; Nazeeruddin, Md. K.; Grätzel, M.; Nelson, J.; Li, X.; Long, N. J.; Durrant, J. R. Molecular Control of Recombination Dynamics in Dye-Sensitized Nanocrystalline TiO_2 Films: Free Energy vs Distance Dependence. *J. Am. Chem. Soc.* **2004**, *126*, 5225−5233.